Absolute and convective instabilities in combined Couette-Poiseuille flow past a neo-Hookean solid

Ramkarn Patne, and V. Shankar

Citation: Physics of Fluids **29**, 124104 (2017);
View online: https://doi.org/10.1063/1.5001132
View Table of Contents: http://aip.scitation.org/toc/phf/29/12
Published by the American Institute of Physics

Absolute and convective instabilities in combined Couette-Poiseuille flow past a neo-Hookean solid

Ramkarn Patne and V. Shankar[a)]
Department of Chemical Engineering, Indian Institute of Technology, Kanpur 208016, India

(Received 22 August 2017; accepted 29 November 2017; published online 29 December 2017)

Temporal and spatio-temporal stability analyses are carried out to characterize the occurrence of convective and absolute instabilities in combined Couette-Poiseuille flow of a Newtonian fluid past a deformable, neo-Hookean solid layer in the creeping-flow limit. Plane Couette flow of a Newtonian fluid past a neo-Hookean solid becomes temporally unstable in the inertia-less limit when the parameter $\Gamma = V\eta/(GR)$ exceeds a critical value. Here, V is the velocity of the top plate, η is the fluid viscosity, G is the shear modulus of the solid layer, and R is the fluid layer thickness. The Kupfer-Bers method is employed to demarcate regions of absolute and convective instabilities in the Γ-H parameter space, where H is the ratio of solid to fluid thickness in the system. For certain ranges of the thickness ratio H, we find that the flow could be absolutely unstable, and the critical Γ required for absolute instability is very close to that for temporal instability, thus making the flow absolutely unstable at the onset of temporal instability. In some cases, there is a gap in the parameter Γ between the temporal and absolute instability boundaries. The present study thus shows that absolute instabilities are possible, even at very low Reynolds numbers in flow past deformable solid surfaces. The presence of absolute instabilities could potentially be exploited in the enhancement of mixing at low Reynolds numbers in flow through channels with deformable solid walls. *Published by AIP Publishing.* https://doi.org/10.1063/1.5001132

I. INTRODUCTION

Fluid flow past deformable solid surfaces has diverse applications ranging from biotransport[1] to microfluidic mixing.[2] In these applications, it is important to understand whether the flow is laminar and when the laminar flow becomes unstable to a more complicated flow. Consequently, stability analysis has been widely used to predict the onset of transition to turbulence in such flows. Kumaran *et al.*[3] studied linear stability analysis of the plane Couette flow past soft surfaces in the creeping-flow limit using the linear viscoelastic model for the deformable solid and predicted the presence of a temporal instability at low, but finite wavenumber (henceforth referred to as the finite-wave instability) which is absent if the walls are rigid.[4] But the linear viscoelastic model is not applicable when finite base state strains are prevalent in the deformable solid because of which the non-linear terms in the strain tensor of the solid become significant. Gkanis and Kumar[5] studied same geometry in the creeping-flow limit, but they used the neo-Hookean model for the solid which introduces a new instability at high wavenumbers (hereafter referred to as "short-wave" instability). This result differs from the linear viscoelastic model in predicting critical parameter values for solid thickness values $H < 1$, but the results remain unchanged for $H > 1$, where H is the ratio of thickness of solid to fluid layers.[5] The presence of the short-wave instability observed by Gkanis and Kumar[5] was attributed to the first normal stress difference in the solid in the base state, which is absent in a linear viscoelastic solid.[3] This characteristic presence of short-wave instability for a neo-Hookean model has also been confirmed for plane Poiseuille[6,7] and tube flows[8] with deformable walls. However, the Lagrangian formulations (for the solid) used in the stability analysis by Gaurav and Shankar[6] and Gkanis and Kumar[7] had inconsistencies in the interface conditions which required a Taylor series expansion of finite base state quantities. Similarly, the Lagrangian formulation of Chokshi and Kumaran[9] was inconsistent because the base quantities were left as a function of the undeformed coordinates instead of pre-stressed state coordinates as dictated by the momentum balance equation for the perturbed state. The above inconsistencies were resolved recently by Patne *et al.*[10] who proposed consistent Eulerian and Lagrangian formulations for the solid which is used in the present study.

There have also been experimental studies which probed the presence of instabilities in flow past deformable solid layers. Kumaran and Muralikrishnan[11] carried out experiments in which a liquid layer is present between two rotating discs of a commercial rheometer, with the bottom disc being coated with a soft polymer gel. They determined the viscosity in the geometry with the soft gel. When the flow is viscometric (i.e., stable laminar flow), they observed that the viscosity in this system is the same as the viscosity of the liquid used. However, beyond a critical strain rate, the observed viscosity strongly deviates from the expected viscosity value of the fluid, and this is taken as a signature of the onset of instability. They compared their experimental results for the critical strain rate for instability with theoretical predictions (obtained using the linear viscoelastic model) and found quantitative agreement with no adjustable parameters for the Couette flow

[a)]Author to whom correspondence should be addressed: vshankar@iitk.ac.in

of a Newtonian fluid past a deformable solid. Experimental studies by Neelamegam *et al.*[12] for plane Couette flow past the two-layer gel also showed an agreement between theoretical predictions (using the neo-Hookean model for the solid) and experimental observations. Verma and Kumaran[13] experimentally studied plane Poiseuille flow with deformable walls and observed that the theoretical predictions (using the neo-Hookean model) and experimental observations for the transition Reynolds number quantitatively agree provided if one considered the stability of the flow in the deformed configuration, as there is a non-negligible alteration of the shape of the deformable tube/channel due to the applied pressure gradient. Neelamegam and Shankar[14] carried out experiments to characterize the onset of instability for Hagen-Poiseuille flow through a tube with deformable walls and found that the scaling predicted by theory (using the neo-Hookean model) and experiments do not agree. Thus, while significant advances have been made on the theoretical front, there still remain some discrepancies between experimental observations and theoretical predictions.

Earlier studies on plane Couette flow past soft surface geometry studied only the temporal evolution of the disturbances and its relevance to experimental studies. However, a temporal stability analysis does not answer the question of how disturbances develop in space and time, i.e., whether the growth of the disturbances is in space or time or in both space and time simultaneously. For studying the evolution of disturbances with respect to time, viz., temporal stability analysis, the frequency of the disturbances, ω, is taken as a complex number and the wavenumber, k, is a real number.[15] For spatial stability analysis, which studies the evolution of disturbances with respect to space, we take ω as a real number and k as a complex number.[4] For studying the development of disturbances with respect to space and time, it is necessary to perform a spatio-temporal stability analysis, where it is necessary to consider both ω and k as complex numbers.[16,17]

The characterization of fluid flows as being absolutely or convectively unstable and the methodology to investigate these phenomena by progressive moving of the contours in the complex frequency and wavenumber plane (discussed in Sec. III) were first proposed by Briggs[18] in context of plasma physics. The presence of an absolute instability signifies the growth of disturbances in both upstream and downstream directions from the point where the disturbance is introduced. This is not the case with convective instability, where disturbances are swept downstream from the source of the disturbance, and given sufficient time these disturbances decay at any fixed position in space.[16] The spatio-temporal evolution of disturbances is best illustrated by considering the response of a given base velocity profile to an impulse excitation in the asymptotic limit of long times.[16] From this asymptotic response, it can be inferred whether the flow is absolutely or convectively unstable. For illustration purposes, consider a linear dispersion relation $\omega = f(k)$, where $f(k)$ is a continuous and differentiable function of k. In order for absolute instability to exist, the group velocity of the disturbances must be zero[16,17] which implies $\frac{\partial \omega}{\partial k} = 0$, but this is not a sufficient condition for absolute instability. The roots of $\frac{\partial \omega}{\partial k} = 0$ are the saddle points of the (linear) dispersion relation. If there is a first-order saddle point in the k-plane (denoted by k_0), then a local Taylor expansion about this point would yield $(\omega - \omega_0) \sim (k - k_0)^2$, where ω_0 is the value of ω at the saddle point k_0. Because of the angle-doubling (i.e., phase doubling) property of this local mapping between ω and k planes, the saddle point (k_0) in the k-plane corresponds to a cusp point (ω_0) in the ω plane. The method described earlier, however, gives a number of saddle points, and to determine the saddle point which obeys the causality principle (which stipulates that the cause does not precede effect), the Briggs-Bers[18] method is needed. Kupfer *et al.*[19] employed this local mapping to conceptualize a simpler method, wherein to predict an absolute instability we need to detect the formation of the cusp point in the ω plane and if this cusp point corresponds to $\mathrm{Im}(\omega) > 0$ and is genuine (as explained in Sec. III), then it can be concluded that the flow is absolutely unstable.

Absolute instability is absent in plane Couette flow past the rigid surface as there is no temporal instability[4] in that flow. Deissler[20] showed the absence of absolute instability for plane Poiseuille flow in a rigid channel although the flow is temporally unstable. Consequently, the presence of an absolute instability (if any) in the present configuration of combined Couette-Poiseuille flow past a deformable surface should then be a consequence of the dynamics of the deformable solid. If absolute instabilities are indeed present in flow past deformable solid walls, then this feature can be exploited in promoting mixing in such flows by varying the parameters (e.g., shear modulus of the solid, dissipation in the solid) such that absolute instability is triggered which can hasten mixing as absolute instabilities are in general catastrophic when compared to convective instabilities. In microfluidic devices fabricated using elastomers, the length of the channel may not be sufficiently long for convective instabilities to grow within the domain of the device. However, if absolute instabilities are present in such devices, then the flow is destabilized in the entire domain of the channel. Thus, there are important practical consequences due to the presence of absolute instabilities in channels with deformable solid walls.

There have been some earlier studies in flow past deformable solid boundaries that characterized convective and absolute instabilities, but most of these studies were for external boundary layer flows past a deformable wall. Carpenter and Garrad[21] classified the instabilities as being fluid-based and solid-based, but Sen and Arora[22] found the presence of instability which is formed by the coalescence of the solid-based and fluid-based unstable modes, which they termed as transitional mode. However, the authors did not conclude whether this transitional mode is absolutely unstable or not. Carpenter and Garrad[21] investigated the presence of absolute instability in the Kramer-type compliant surfaces, while Yeo *et al.*[23–25] used a continuum linear viscoelastic model for the solid to analyze boundary layer flow over such deformable walls. They used the Kupfer-Bers method[19] and found the boundary layer flow past a viscoelastic solid to be absolutely unstable, which is not the case in the boundary-layer flow over rigid surfaces. Hamadiche and Gad-el-Hak[26] carried out spatio-temporal stability analysis of Hagen–Poiseuille flow of a Newtonian fluid in an incompressible, collapsible, viscoelastic tube for axisymmetric and non-axisymmetric

disturbances. For axisymmetric disturbances, they found the presence of two convectively unstable modes of which, one was propagating upstream while the other one propagating downstream. For non-axisymmetric disturbances, there was an upstream propagating absolutely unstable mode. The existence of absolute instability for blood-vessel-like geometries was studied by Hamadiche *et al.*[27] where they considered a three-layered wall made up of soft material with different rheological properties. Hamadiche *et al.*[27] showed that it is possible to convert absolute instability to convective instability and vice-versa by varying the rheological parameters of the three solid layers.

In the present study, we have considered the neo-Hookean solid model for studying spatio-temporal stability analysis of flow past a deformable solid. The flow considered here is the combined plane Couette-Poiseuille flow past a neo-Hookean solid. Due to the use of a neo-Hookean model, there is a normal stress difference in the solid in the base state, which becomes the reason for the presence of short-wave (high-wavenumber) instability. As we demonstrate in this work, this characteristic short-wave instability in the neo-Hookean solid plays an important role in the existence of absolute instabilities. The rest of the paper is structured as follows: Sec. II discusses the formulation of the problem by using the Lagrangian formulation for the solid. A brief discussion on the analysis of absolute and convective instabilities is provided in Sec. III. Results from temporal and spatio-temporal stability analysis of the flow under consideration are discussed in Sec. IV. The salient conclusions of the present study are summarized in Sec. V.

II. PROBLEM FORMULATION

We consider an incompressible Newtonian fluid with viscosity η and density ρ is flowing through a channel of width R past a neo-Hookean solid of dimensional thickness HR (where H is the non-dimensional solid thickness) bonded to rigid solid, with shear modulus G and density ρ. A combined Couette-Poiseuille flow is considered in this channel where the Couette flow component is created by moving the upper plate at steady (dimensional) velocity V and the Poiseuille flow component is due to an applied pressure gradient. We non-dimensionalize lengths, velocity, pressure and stresses with respect to R, GR/η and G, respectively. Let $\mathbf{v} = (v_x, v_z)$ denote the velocity field, where v_x and v_z, are, respectively, velocities in the x and z directions. The schematic of the geometry (in non-dimensionalized coordinates) for the problem is shown in Fig. 1, where x is the flow direction and z is the direction perpendicular to the flow.

Then the continuity equation is given by

$$\nabla \cdot \mathbf{v} = 0. \tag{1}$$

The Navier-Stokes momentum equation takes the form

$$\frac{Re}{\Gamma}\left(\frac{\partial \mathbf{v}}{\partial t} + (\mathbf{v}\cdot\nabla)\,\mathbf{v}\right) = -\nabla p + \nabla^2 \mathbf{v}. \tag{2}$$

Here, p is the pressure in the fluid, $Re = \rho R V_{avg}/\eta$ is the Reynolds number, and $\Gamma = \eta V_{avg}/GR$, is the dimensionless velocity with V_{avg} as the average velocity of the base flow.

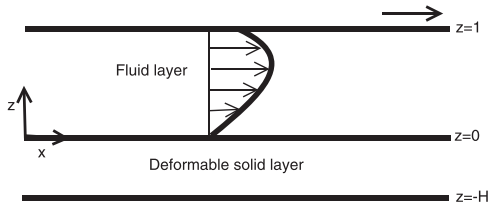

FIG. 1. Schematic of the flow geometry. The upper plate moves with non-dimensional steady velocity of $2\Gamma_{Couette}$, where $\Gamma_{Couette}$ is the nondimensional average velocity of the Couette component of the flow. The figure shows the velocity profile for $\frac{d\bar{p}}{dx} < 0$. The nondimensional coordinates x and z are scaled with the thickness of the fluid layer.

The non-dimensionalised base state velocity profile is

$$\bar{v}_x = \Gamma\left[(6-4\,\epsilon)z - 6\,(1-\epsilon)\,z^2\right], \tag{3}$$

where the overbar indicates base state variable. Henceforth, base state quantities will be indicated by an overbar except for $\bar{\mathbf{x}}$, which denote pre-stressed state coordinates for the solid. The pressure gradient in the flow direction is

$$\frac{d\bar{p}}{dx} = -12\,\Gamma\,(1-\epsilon), \tag{4}$$

where $\epsilon = \Gamma_{Couette}/\Gamma$, with $\Gamma_{Couette}$ as the dimensionless average velocity of Couette flow. The velocity profile is obtained such that the volumetric flow rate remains same while we change parameter ϵ, so that critical parameter values required for instability can be compared. The limiting cases of the various values of ϵ can be summarized as follows:

$$\epsilon = 1, \qquad \text{Couette flow}, \tag{5}$$

$$0 < \epsilon < 1, \quad \text{Couette-Poiseuille flow}\left(\frac{d\bar{p}}{dx} < 0\right), \tag{6}$$

$$\epsilon = 0, \qquad \text{Poiseuille flow}, \tag{7}$$

$$\epsilon > 1, \quad \text{Couette-Poiseuille flow}\left(\frac{d\bar{p}}{dx} > 0\right). \tag{8}$$

For the solid, consider a representative particle with the position vector $\mathbf{X} = (X_1, X_2, X_3)$ in the undeformed solid. Assuming the solid to be incompressible and letting fluid flow past it, the representative particle will now assume the position vector, $\mathbf{x} = (x_1, x_2, x_3)$. The current and undeformed position vectors are related by

$$\mathbf{x}(\mathbf{X}) = \mathbf{X} + \mathbf{u}(\mathbf{X}), \tag{9}$$

where $\mathbf{u}(\mathbf{X})$ is the Lagrangian displacement in the solid. Hence the deformation gradient is, $\mathbf{F} = \frac{\partial \mathbf{x}}{\partial \mathbf{X}}$. The incompressibility condition is given by

$$\det(\mathbf{F}) = 1. \tag{10}$$

The dimensionless Cauchy stress for a purely elastic neo-Hookean solid is[10,28,29]

$$\boldsymbol{\sigma} = -p_g \mathbf{I} + \mathbf{F}\cdot\mathbf{F}^T, \tag{11}$$

with p_g being the pressure field in the solid. The non-dimensionalised momentum balance equation[28,30] is

$$\frac{Re}{\Gamma}\frac{\partial^2 \mathbf{u}}{\partial t^2} = \nabla_{\bar{\mathbf{x}}} \cdot \mathbf{P}, \tag{12}$$

$$\mathbf{P} = \mathbf{F}^{-1} \cdot \boldsymbol{\sigma}, \tag{13}$$

where $\mathbf{P}$ is the first Piola-Kirchhoff stress tensor. At the rigid solid-neo-Hookean solid interface ($\bar{z} = -H$), there will be no perpendicular or tangential motion as it is assumed that the neo-Hookean solid is perfectly bonded to the rigid solid. Hence, the boundary condition at this interface becomes $\mathbf{u} = 0$. At the fluid-solid interface, continuity conditions are imposed for the velocity and stresses. In the base state, the motion is, $\bar{\mathbf{x}}(\mathbf{X}) = \mathbf{X} + \bar{\mathbf{u}}(\mathbf{X})$, which leads to the base state deformation gradient $\bar{\mathbf{F}} = \frac{\partial \bar{\mathbf{x}}}{\partial \mathbf{X}}$. Substituting $\bar{\mathbf{F}}$ in Eqs. (10)–(13), and following the procedure outlined by Patne *et al.*[10] the steady base state the deformation in the solid in terms of the pre-stressed state coordinates is

$$\bar{u}_x = 6\,\Gamma\,(1-\epsilon)\,(H^2 - \bar{z}^2) + \Gamma\,(6-4\,\epsilon)\,(\bar{z}+H). \tag{14}$$

Similarly, the base state pressure in the solid is

$$\bar{p}_g = -12\,\Gamma\,(1-\epsilon)\,\bar{x}. \tag{15}$$

For the perturbed state, the motion is described by $\mathbf{x}(\bar{\mathbf{x}}) = \bar{\mathbf{x}} + \mathbf{u}'(\bar{\mathbf{x}}, t)$. Here, $\mathbf{u}'(\bar{\mathbf{x}}, t)$ is the Lagrangian displacement of the particle from base state, and the prime indicates that it is a perturbation quantity (henceforth, perturbation quantities will be indicated by a prime). The deformation gradient becomes $\mathbf{F} = \frac{\partial \mathbf{x}}{\partial \bar{\mathbf{X}}}$. The incompressibility condition for the perturbed state after using the base state incompressibility condition becomes $det(\mathbf{F}') = 1$. Further, we take the creeping-flow limit in this study and assume two-dimensional disturbances with normal modes of the form

$$(v_x', v_z', p')(\mathbf{x}, t) = (\tilde{v}_x, \tilde{v}_z, \tilde{p})(z)\, e^{i\,k\,(x-ct)}, \tag{16}$$

$$(u_x', u_z', p_g')(\bar{\mathbf{x}}, t) = (\tilde{u}_x, \tilde{u}_z, \tilde{p}_g)(\bar{z})\, e^{i\,k\,(\bar{x}-ct)}, \tag{17}$$

where k is the wavenumber in the z direction, while $c = c_r + ic_i$ is the complex velocity of the perturbations with c_r as the phase speed and c_i as the growth or decay rate of the perturbations. Hence flow will be unstable if for any eigenvalue $c_i > 0$. It must be noted that a tilde over a quantity indicates the eigenfunction or the Fourier transform of the corresponding perturbation quantity. The governing equations for the fluid can be written as

$$ik\tilde{v}_x + D\tilde{v}_z = 0, \tag{18}$$

$$-ik\tilde{p} + (D^2 - k^2)\,\tilde{v}_x = 0, \tag{19}$$

$$-D\tilde{p} + (D^2 - k^2)\,\tilde{v}_z = 0, \tag{20}$$

where $D = \frac{d}{dz}$. Similarly for the solid, the incompressibility condition is

$$ik\tilde{u}_x + D\tilde{u}_z = 0, \tag{21}$$

and momentum balance equations are

$$-ik\tilde{p}_g + \left(D^2 + 2ikD\bar{u}_x D - k^2(1 + (D\bar{u}_x)^2) + ik\,D^2\bar{u}_x\right)\tilde{u}_x - D_{\bar{x}}\bar{p}_g D\tilde{u}_z = 0, \tag{22}$$

$$-D\tilde{p}_g + \left(D^2 + 2ikD\bar{u}_x D - k^2(1 + (D\bar{u}_x)^2) + ik\,D^2\bar{u}_x\right)\tilde{u}_z + D_{\bar{x}}\bar{p}_g D\tilde{u}_x = 0, \tag{23}$$

where $D = \frac{d}{d\bar{z}}$ and $D_{\bar{x}} = \frac{d}{d\bar{x}}$. The above equations are quite general and can be used for any planar flow geometry provided that we specify $\bar{u}_x(\bar{z})$ and $\bar{p}_g(\bar{x})$. The above equations for the fluid and solid are then solved by using the following boundary conditions. At $z = 1$, i.e., at the upper plate, the absence of slip and permeability implies

$$\tilde{v}_x = 0, \quad \tilde{v}_z = 0. \tag{24}$$

At $z = 0$, i.e., at the fluid-soft solid interface, velocity and stress continuity gives

$$\tilde{v}_z = -ikc\tilde{u}_z, \tag{25}$$

$$\tilde{v}_x + D\bar{v}_x\tilde{u}_z = -ikc\tilde{u}_x, \tag{26}$$

$$D\tilde{u}_x + ik\tilde{u}_z + 12\Gamma(1-\epsilon)\tilde{u}_z = D\tilde{v}_x + ik\tilde{v}_z, \tag{27}$$

$$-\tilde{p}_g + 2\,(ikD\bar{u}_x + D)\tilde{u}_z - 12\Gamma(1-\epsilon)\tilde{u}_x = -\tilde{p} + 2D\tilde{v}_z - Tk^2\tilde{u}_z, \tag{28}$$

where T is the dimensionless interfacial tension. At $z = -H$, as the deformable solid is perfectly bonded to the rigid solid, the displacement of the deformable solid will be zero, i.e.,

$$\tilde{u}_x = 0, \quad \tilde{u}_z = 0. \tag{29}$$

The continuity and momentum balance equations for the fluid and solid are to be solved by using the above boundary conditions. As the differential equations have coefficients which are the functions of z, an analytical solution is not possible. Hence we numerically integrate fluid perturbation governing equations from the upper plate ($z = 1$) upto the interface by utilizing boundary conditions (24). Similarly for the solid, perturbation governing equations are numerically integrated from ($z = -H$) by using boundary conditions (29). The eigenfunctions obtained above are then used in the interface conditions (25)–(28) to form a matrix which is then solved for the eigenvalue (c) for the given values of the parameters. The numerical integration is performed by using the *ode45* package of MATLAB.

III. ANALYSIS OF ABSOLUTE AND CONVECTIVE INSTABILITIES

The linear spatio-temporal response of an initially localised disturbance at $x = 0$ and $t = 0$ can be analyzed by considering the evolution of Green's function provided the given disturbance is an impulse function. The expression for Green's function is

$$G(x,t) = \int_F \int_L \frac{e^{i(kx-\omega t)}}{D[k,\omega;R]} d\omega dk, \tag{30}$$

where F is the Fourier contour in the k (complex wavenumber)-plane and L is the Laplace contour in the ω (complex frequency)-plane and R is the system parameter. Also $D[k, \omega; R]$ is the (linear) dispersion relation which relates k and ω, and as discussed in Sec. I this dispersion relation is used to obtain the saddle points. For integrating the above integral, the L-contour must be placed above all singularities of the dispersion relation $D[k, \omega; R]$ in the ω-plane so that the causality is not violated and F-contour must be placed in the

k-plane such that it will be along the k_r-axis.[16] To obtain the spatio-temporal evolution of the disturbances, the evaluation of the above integral is necessary, but this is not generally feasible. Furthermore, in the understanding of instability, we need the system response at large times where an analytical solution is possible. This involves deforming the contour in the k-plane to make it pass through the saddle point, and the integration can be accomplished by using the method of the steepest descent.[31,32] This gives an expression for Green's function in the asymptotic limit of long times,

$$G(x,t) \sim -(2\pi)^{-1/2} \frac{e^{i[\pi/4+k_0 x-\omega(k_0)t]}}{\frac{\partial D}{\partial \omega}[k_0,\omega(k_0)]\left[\frac{d^2\omega}{dk^2}(k_0)t\right]^{1/2}}, \tag{31}$$

where k_0 is the position of the saddle point in the k plane and $\omega(k_0)$ is the position of the cusp point in the ω plane corresponding to the saddle point k_0. From Eq. (31), one can easily infer the condition for which the system will be absolutely unstable or convectively unstable. For convectively unstable systems,

$$\lim_{t\to\infty} G(x,t) = 0, \quad \text{along the ray } x/t = 0, \tag{32}$$

and for absolutely unstable systems,

$$\lim_{t\to\infty} G(x,t) = \infty, \quad \text{along the ray } x/t = 0. \tag{33}$$

To confirm the presence of absolute instability, the group velocity defined as $\partial\omega/\partial k$, must be zero at the saddle point k_0.

The vanishing characteristic of group velocity at the saddle point is a necessary but not a sufficient condition for the existence of absolute instability. This is because the group velocity is zero at every saddle point or where the two k-branches meet independent of whether the branches originate from same half of the k-plane or not. To overcome this inadequacy, Briggs[18] developed the idea of tracking the F-contour deformation in the k-plane and its relation to the L-contour deformation in the ω-plane by using the analytic continuation. As the contours are deformed, a *pinch point* appears in the k-plane when the two branches intersect ("pinch") each other in the k-plane. Concurrently, a *cusp point* appears in the ω-plane which is a branch-point. Further deformation of the contours after the pinch point is formed violates causality, and the deformation of the contours is stopped. In the present work, we encounter only a second-order algebraic branch point in the ω-plane and a first-order saddle point in the k-plane as discussed in Sec. IV B.

To ascertain whether the detected cusp point is formed due to the analytic continuation of the k-branches originating from the different halves of the k-plane or not, the following procedure is adopted. Following Ref. 19, we can either draw a straight ray from the cusp point such that it will intersect the image of the F-contour (for $k_i = 0$) in the ω-plane and then count the number of times such intersections occur or count the number of times both k-branches cross the k_r-axis before forming pinch point in the k-plane. If either one or both of the k-branches have crossed the k_r-axis even number of times or the ray drawn from the cusp point in the ω-plane intersects the image of the F-contour (for $k_i = 0$) in the ω-plane even number of times, then the observed cusp point is formed due to k-branches originating from same half of the k-plane,[19] and this scenario corresponds to an *evanescent mode*.[23] If the count of intersections by the straight line with the image of the F-contour (for $k_i = 0$) in the ω plane turns out to be odd, then the observed cusp point is formed due to the two k-branches originating from different halves of the k-plane and the concerned cusp point is termed as genuine. If this genuine cusp point is formed in the upper half of the ω-plane, i.e., if $\omega_i > 0$, then the system is absolutely unstable. If $\omega_i < 0$, the flow is convectively unstable, provided it is already temporally unstable; otherwise, the system is stable.

The absolute instability is far more dangerous than the convective instability as the occurrence of absolute instability will pervade the entire flow domain, i.e., both in the direction of the flow and in the direction opposite to the flow. This *resonance* of the upstream and downstream eigenmodes at the disturbance source leads to growth as long as the cusp point is located in the upper half of the ω-plane. However, for convectively unstable systems, the disturbance is convected away from the source as time progresses hence leaving the flow domain as such if given sufficient time. However, convective instability can cause transition to turbulence if a sufficient spatial distance is given for the disturbances to grow. Kupfer *et al.*[19] developed a method by exploiting the local map relationship $(\omega - \omega_0) \sim (k - k_0)^2$ which considerably reduces the task of finding an absolute instability because the dispersion relations that are found for practical problems are usually transcendental in k and algebraic in ω. Hence it becomes difficult to find k for a given ω and is usually quite computationally intensive. But, in the Kupfer-Bers method, we consider only the formation of a cusp point in the ω-plane. From the local map relation, it can be easily inferred that the angle doubling property is an essential feature of the formation of branch point singularity in the ω-plane provided that the pinch point corresponding to this cusp point is a first-order saddle point. Here we will restrict ourselves only to first-order saddle points as only such points are encountered in the present work.

In the Kupfer-Bers[19] method, we scan a certain region in the k-plane using a contour with different values of $k_i < 0$ and varying k_r, and the images of this contour is plotted in the ω-plane. For a particular k_i contour, the cusp point appears. After locating the cusp point, in order to confirm that it is indeed genuine, the procedure outlined above based on the construction of a ray from the cusp point is adopted. During our analysis, we also encountered "evanescent modes" and a schematic example of how the evanescent mode differs from a genuine mode is given below. Consider the formation of the branch point in the ω-plane as shown in Fig. 2.[23] The ray, shown with a thin line intersects $k_i = 0$ image even number of times. This means that the cusp point formed is not genuine and hence corresponds to an evanescent mode. This can also be interpreted as the double crossing by a k-branch of the k_r-axis, so the saddle point forming branches originate from the same half-plane of the k-plane.[23]

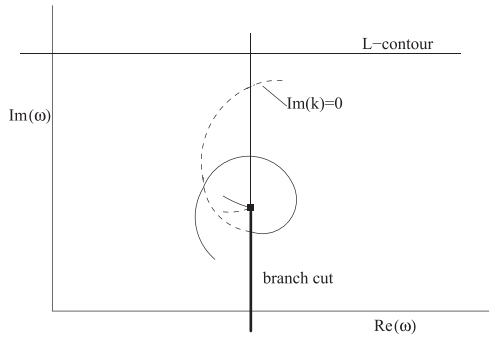

FIG. 2. Evanescent mode formation in the ω-plane (thick line is branch cut).

IV. RESULTS AND DISCUSSION

A. Temporal stability analysis

The temporal stability analysis of the combined Couette-Poiseuille flow past a neo-Hookean surface was first studied by Gkanis and Kumar,[7] but owing to the use of inconsistent interface conditions some of the conclusions obtained in their work need to be revisited. In the present work when the consistent interface conditions are used, we show that the finite-k instability predicted by Gkanis and Kumar[7] is absent in the creeping-flow limit for plane Poiseuille flow. Figure 3 shows the effect of variation in ϵ, i.e., variation of the pressure gradient on the temporal stability. As can be observed from Fig. 3, as the pressure gradient is increased in the flow direction, finite-wave disturbances are stabilized while short-wave disturbances are destabilized. This stabilisation and destabilisation phenomena will be further discussed in Fig. 7. For positive pressure gradients ($\epsilon > 1$), forces acting on the solid due to the Couette and Poiseuille components of the flow will be in opposite directions. As explained later, this leads to the presence of finite-wave instability which is shown in Fig. 3 for $\epsilon = 1.2$. Similar to the prediction of Gaurav and Shankar,[6] we too find that the finite wave instability is absent in the creeping flow limit for Poiseuille flow past a neo-Hookean solid (Fig. 4).

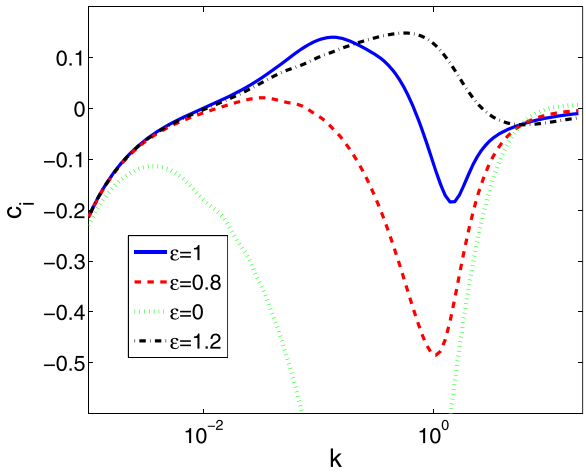

FIG. 3. Results from the temporal stability analysis: c_i vs k for different values of ϵ for $H = 10$, $\Gamma = 1$, and $T = 0$. The figure shows stabilizing and destabilizing effects of variation in ϵ.

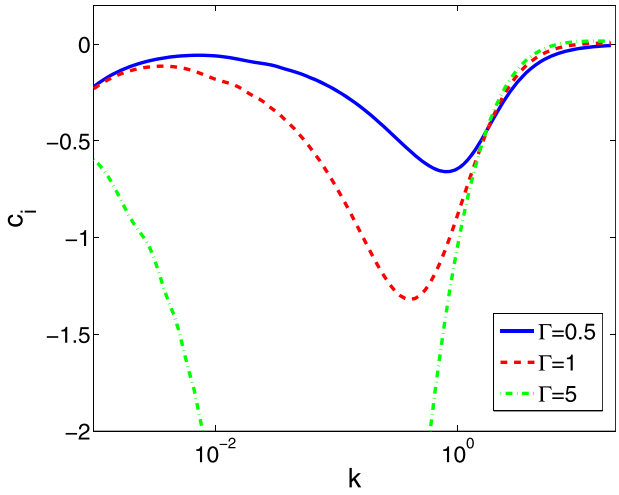

FIG. 4. Results from the temporal stability analysis: c_i vs k for different values of Γ for $H = 10$, $\epsilon = 0$, $T = 0$. This figure illustrates the absence of finite-wave instability observed for plane Poiseuille flow past a neo-Hookean solid.

To analyze the stability behavior further, it is necessary to understand the effect of change in the pressure gradient on the critical parameters and possible qualitative changes in the type of the instabilities observed. Hence in Fig. 5, neutral curves for varying values of ϵ are plotted for $H = 0.5$. The plot shows only the presence of short-wave instability for $\epsilon = 0$ and 1, which, respectively, denote plane Poiseuille and Couette flows. However, for $\epsilon = 1.4$ (i.e., combined Couette-Poiseuille flow), the neutral curve has characteristics of the finite-wave instability such as a nearly parabola-shaped neutral stability curve and, as shown later, the critical value of Γ for the flow to be temporally unstable (Γ_{ct}) scales as $\Gamma_{ct} \sim \frac{1}{H}$. Thus, surprisingly while both plane Couette and plane Poiseuille flows do not exhibit finite wave instability for $H = 0.5$, the combined Couette-Poiseuille flow exhibits a finite wave instability for $\epsilon = 1.4$. Physically, this may be rationalized as follows: For $\epsilon > 1$, the Couette and Poiseuille flows are in the opposite

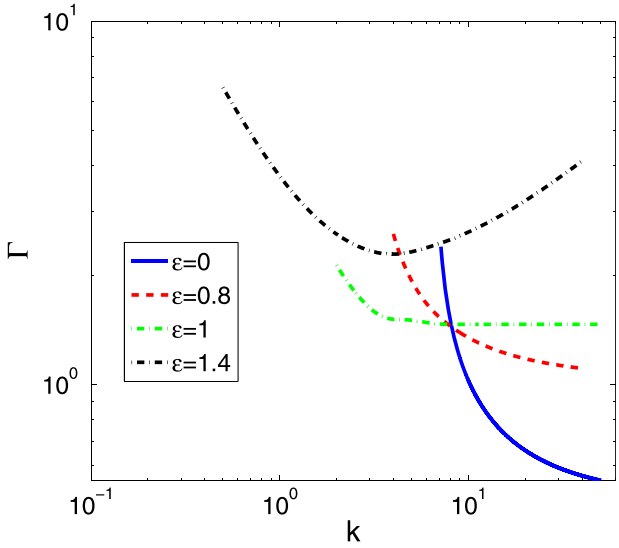

FIG. 5. Neutral stability curves for the combined Couette-Poiseuille flow in the Γ–k parameter space for $H = 0.5$ and $T = 0$. This figure shows the presence of the finite-wave instability for $\epsilon = 1.4$.

directions, and because of this the velocity gradient of the base state flow at the fluid-solid interface decreases with the increase in ϵ for $\epsilon > 1$. As the base-state deformation field in the solid is dictated by the shear stresses exerted by the fluid at the fluid-solid interface, when the velocity gradient of the base flow becomes smaller, the deformation induced in the solid also becomes smaller. In that limit, the neo-Hookean solid behaves almost like a linear elastic solid as the base-state strains induced in the solid are sufficiently small. For linear elastic solids,[3,33] the finite wave instability is always present in the creeping-flow limit regardless of the flow (i.e., plane Couette or plane Poiseuille). Thus, the combined Couette-Poiseuille flow past a neo-Hookean solid exhibits a finite wave instability for $\epsilon > 1$, and the neo-Hookean solid effectively behaves like a linear elastic solid. For the same reason, the first-normal stress difference becomes negligible in the neo-Hookean solid, and the short-wave instability is not present for $\epsilon > 1$. This is further illustrated in Fig. 6 where we plot the variation of the critical strain rate for temporal instability, Γ_{ct}, with solid thickness H. For $H < 1$, the curve for $\epsilon = 1.2$ shows characteristics of the finite-wave instability, with $\Gamma_{ct} \propto 1/H$ for all values of H.

From Fig. 6, it is also clear that Γ_{ct} is constant with respect to the variation in H for $\epsilon = 0$ (viz., plane Poiseuille flow), and this is due to the presence of only short-wave instability which is independent of H. For $\epsilon = 0$, the critical strain rate $\Gamma_{ct} \sim 0.5$ even though only short-wave instability is present. It must be noted that earlier studies in the creeping-flow limit for flows past a neo-Hookean solid observed a short-wave instability only for $\Gamma > 1$. The reason for $\Gamma_{ct} < 1$ for the short-wave instability in the present work is because of using the entire channel width as the length scale and average velocity as the velocity scale for nondimensionalization. If instead we use the half channel width and maximum velocity for plane Poiseuille flow, the results are in agreement with Ref. 6. The curves for $\epsilon = 0.8, 1.2$ which represent combined Couette–Poiseuille flow show the effect of the pressure gradient on the finite-wave and short-wave instabilities. It must be noted that for $\epsilon = 0.8$, from Eq. (4), the pressure gradient will be negative for positive values of Γ and hence Couette flow and Poiseuille flow will be in the same direction, while for the case of $\epsilon = 1.2$, the pressure gradient will be positive, creating Poiseuille flow which will be in the opposite direction to that of the Couette flow. Comparison of the results for $\epsilon = 0.8$ and $\epsilon = 1$ (viz., Couette flow), shows a decrease in Γ_{ct} for the values of H for which either only short-wave instability exists or it becomes unstable before the finite-wave instability. To conclude, if the pressure gradient is negative and if the magnitude of this pressure gradient increases, this has a destabilizing effect on the short-wave instability. Similar comparison of curves for $\epsilon = 1$ and $\epsilon = 1.2$ shows that an increase in the pressure gradient has a stabilizing effect for lower H and higher H values, while destabilizing effect for intermediate H values. The above picture becomes clearer in Fig. 7, where the variation of Γ_{ct} with ϵ for representative values of H is shown. Gkanis and Kumar[7] also studied the same parameter space, but owing to the inconsistent base state and boundary conditions, their plots differ from the present results. One of the most interesting differences is the absence of any instability for $\epsilon = 1.5$ for any value of H. This absence of instability can be deduced from Eq. (14). The stress acting on the solid due to the fluid motion at the solid-fluid interface is

$$\frac{d\bar{u}_x}{d\bar{z}} = \Gamma\,(6 - 4\,\epsilon). \tag{34}$$

Equating Eq. 34 to zero gives $\epsilon = 1.5$, i.e., there will be no stress acting on the solid even though there is fluid flow. This particular value of ϵ indicates a perfect cancellation of the shear stresses at the fluid-solid interface caused by Couette and Poiseuille flows, so that the base-state deformation in the solid is zero. This value of ϵ also makes the interaction between base and perturbed states in the tangential velocity balance zero, and this removes any energy transfer from base state to perturbations which is necessary for triggering the instability. Although there are similar types of interaction terms in stress continuity conditions, this interaction is not sufficient to cause an instability in the creeping-flow limit. Further, for $\epsilon < 0.7$, $H = 10$ and for $\epsilon < 0.8$, $H = 3$, the results overlap with those

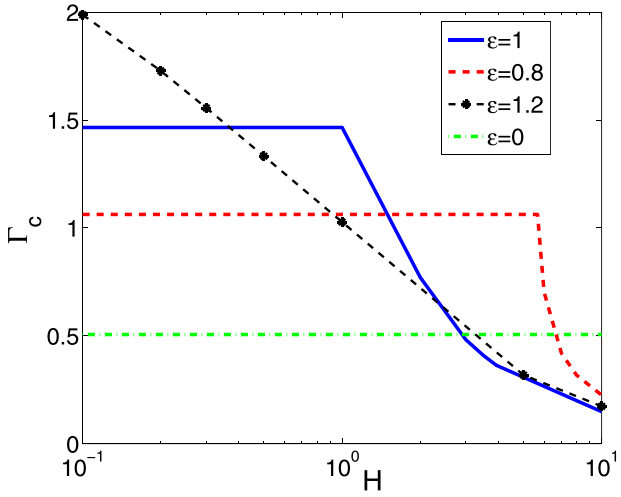

FIG. 6. Combined Couette-Poiseuille flow: H vs Γ_{ct} for different values of ϵ and $T = 0$, showing effect of positive and negative pressure gradients on the temporal stability.

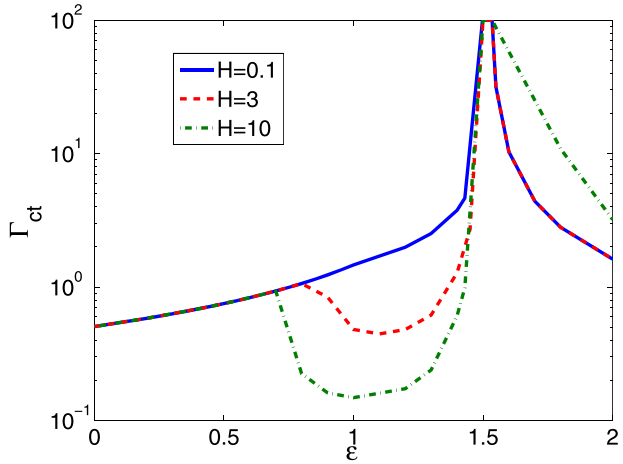

FIG. 7. Variation of Γ_{ct} with respect to ϵ for $H = 0.1$, 3, and 10 for combined Couette-Poiseuille flow.

for $H = 0.1$. This is because of the presence of only short-wave instability for all values of H. The departure of the curve for $H = 10$ from $H = 0.1$ for $\epsilon > 0.7$ is because of the dominance of the finite-wave instability in determining the stability of the system. A similar case is observed for the $H = 3$ curve, but the departure of the curve is delayed, indicating an increase in influence of short-wave instability as the H value is decreased. Also the $H = 3$ curve does not coincide with the $H = 10$ curve for $\epsilon > 0.8$ as Γ_c for the finite-wave instability is inversely proportional to H. This also explains the location of the curve for $H = 3$, which lies between the curves for $H = 0.1$ and $H = 10$.

The effect of interfacial tension on the stability is shown in Fig. 8. It has been observed in previous studies[5,6] that interfacial tension has stabilizing effect on the short-wave instability. Our results show that the effect of the interfacial tension to be more prominent as ϵ is decreased from 1 to 0 due to the increasing dominance of the short-wave instability.

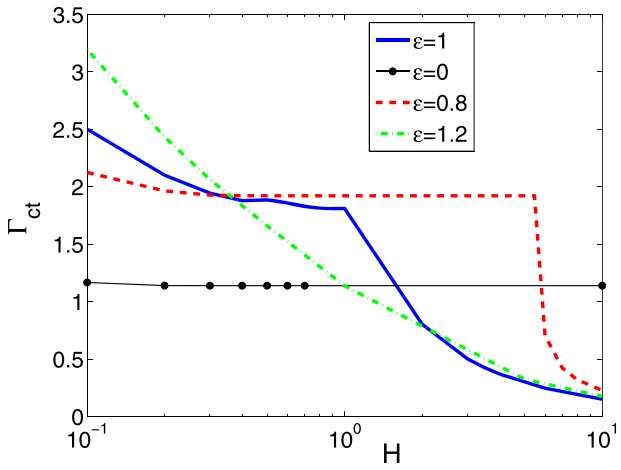

FIG. 8. Role of nonzero interfacial tension at the solid-fluid interface in combined Couette-Poiseuille flow. H vs Γ_{ct} for different values of ϵ, for $T = 0.5$.

B. Spatio-temporal stability analysis

1. Plane Couette flow

In Sec. IV A, we discussed results from the temporal stability analysis where c was taken to be a complex number and k to be a real number. In this subsection, we take both c and k as complex numbers which is necessary for performing the spatio-temporal stability analysis. Further we use the complex frequency $\omega = ck$ instead of the wavespeed c. Before presenting results, it is first important to demonstrate that the cusp-point in the ω-plane and the saddle-point in the k-plane correspond to each other due to angle doubling property of the local map as stated by Kupfer *et al.*[19] for a first-order saddle point. To this end, a particular set of parameters is considered for which the flow is absolutely unstable ($H = 1.5$, $\Gamma = 2$, $\epsilon = 1$, and $T = 0$). As per the Kupfer-Bers method, first the image of the dispersion relation for $k_i = 0$ is obtained, which corresponds to the temporal stability result. Then we decrease k_i values, and the corresponding images in the ω plane are obtained. When k_i becomes sufficiently negative ($-0.037\,064$ in this case), we observe the appearance of a cusp point in Fig. 9 at $\omega = 0.4032 + 0.030\,48i$. The pinch (saddle) point in the k-plane corresponding to the cusp point in the ω plane appears at at $k = 0.4847 - 0.037\,064i$ as shown in Fig. 10. This was obtained by drawing isocontours of ω_r and ω_i in the k-plane. We next draw a ray from the cusp point and extend it to the temporal curve. Since the ray from the cusp point intersects the temporal curve only once, this implies that the cusp point is genuine.[19,23]

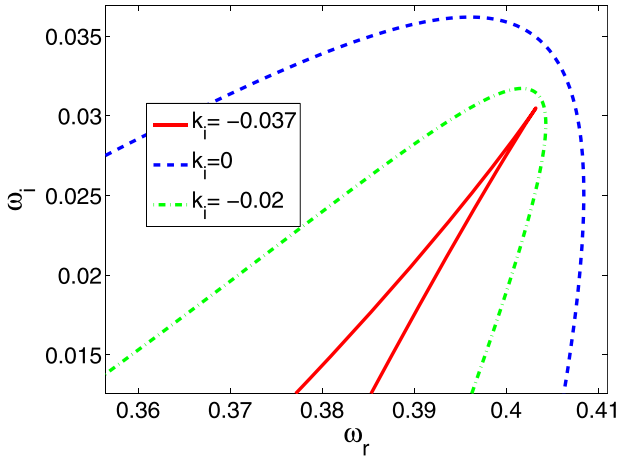

FIG. 9. Cusp point in the ω-plane for $H = 1.5$, $T = 0$, $\Gamma = 2$ for plane Couette flow ($\epsilon = 1$). The cusp point is formed at $\omega = 0.4032 + 0.030\,48i$ for $k_i = -0.037\,064$ and varying k_r.

We also encounter evanescent modes in our study and to illustrate their existence we consider parameters $H = 0.6$, $\Gamma = 1.9$, $T = 0$, and $\epsilon = 1$. Figure 11 shows the formation of the cusp point for this parameter set. However, for this cusp point, the ray drawn from the cusp point intersects the temporal curve in the ω-plane (the curve corresponding to $k_i = 0$) twice (i.e., even number of times), and hence the cusp point corresponds to an evanescent mode. Further analysis of the evanescent modes will not be considered here. For more discussions on evanescent modes the reader is referred to the studies of Lingwood,[34] Koch,[35] and Lundbladh *et al.*[36]

In order to determine the range of Γ for which the system is absolutely unstable (for fixed T, ϵ, and different H), we plot in Fig. 12 the absolute growth rate (the growth rate at the cusp point ω_{i0}) as a function of Γ. From such plots, we arrive at the regions where the flow is convectively unstable or absolutely unstable. We define Γ_{ca} as the minimum Γ required for the flow to be absolutely unstable. Clearly $\Gamma_{ca} \geq \Gamma_{ct}$ where Γ_{ct} is the minimum Γ required for the flow to be temporally unstable. As can be observed from Fig. 12, the flow does not become absolutely unstable for $H = 5$ for any value of Γ. For $H = 3.9447$, initially as Γ is increased, the ω_{i0} value also increases, and at $\Gamma = 0.8$ it shows absolute instability, but on further increment in Γ, the flow is only convectively unstable. The value $H = 3.9447$ is special as the system becomes absolutely unstable for only one value of Γ. For $H = 3.8$, the flow is absolutely unstable for a range of Γ, but for $\Gamma > 1.13$ it becomes convectively unstable. For $H = 1$, initially the system is convectively unstable, but on further increment in Γ, it becomes absolutely unstable, and in this case, it remains absolutely unstable for higher values of Γ.

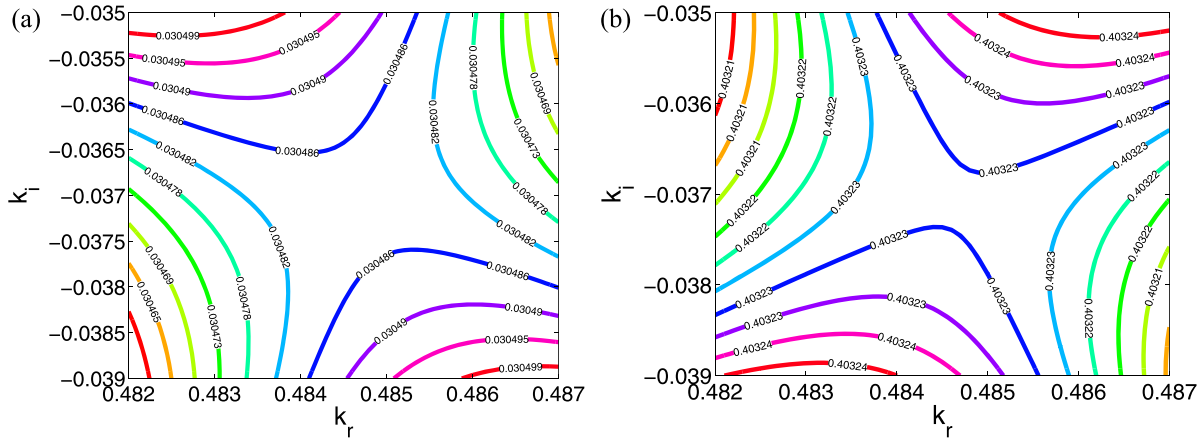

FIG. 10. Pinch (saddle) point in the k-plane corresponding to the cusp point in Fig. 9 for $H = 1.5$, $\Gamma = 2$, and $\epsilon = 1$, $T = 0$. The pinch point at $k = 0.4847 - 0.037\,064i$ in the k plane is formed when $\omega_r = 0.4032$ and $\omega_i = 0.030\,48$. Both panels (a) and (b) demonstrate that the saddle point in the iso-contours of ω_r and ω_i occurs at the same location in the k_r-k_i plane.

Following the same procedure for different values of H, we show the boundaries for absolute and convective instabilities in Fig. 13. In this figure, the legends A, C, E, and S denote, respectively, absolutely unstable, convective unstable, evanescent, and temporally stable regions. Here Γ_{ca} denotes the critical value of Γ for which the system undergoes transition from convectively unstable flow to absolutely unstable flow. Interestingly, at values of $H > 1$, while the temporal stability boundary scales as $\Gamma_{ct} \sim 1/H$, however, the absolutely unstable regions do not necessarily follow this scaling, and depending on the value of H, both absolutely and convectively unstable regions are found in this regime. For $H > 3.94$, there is no absolute instability in the system, and it is not possible for the system to support globally absolutely unstable modes.[16] For $H < 3.94$, this pathway is one of the possibilities, as the system may get into a non-linear region caused due to convectively unstable modes if Γ is not sufficiently high, as there is a small gap in the boundaries for temporal and absolute instabilities.[34] To ascertain this rigorously, a full non-linear analysis is required. However, this generalization is not true for some values of H where short-wave instability governs the stability behavior of the system and $\Gamma_{ct} = \Gamma_{ca}$, showing that absolute instability is the mode of instability, and the system can support global absolutely unstable modes.

An interesting "causality competition" between finite-wave mode and short-wave mode is observed while finding absolute instability for $H < 0.71$. For $H < 0.71$, it is the finite-wave mode that forms the cusp-point first as the Fourier contour is moved in the k-plane and which is convectively unstable for low Γ but is causally legitimate. On further increment in Γ, both finite-wave and short-wave modes form cusp-points at the same k_i, showing both cusps are causally legitimate such that finite-wave mode is convectively unstable while short-wave mode is absolutely unstable. Hence, when the system becomes absolutely unstable, the value of ω_i is quite high, and the instability is catastrophic. But on further increment in Γ, it is the short-wave mode that becomes causally legitimate, and it happens to be an absolutely unstable or evanescent mode. Also, the presence of an evanescent mode is denoted in Fig. 13 as A+E. In this region, depending on the parameters

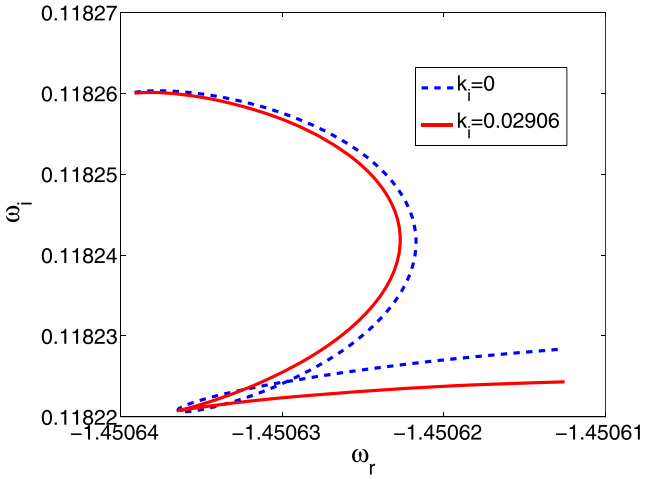

FIG. 11. Evanescent mode formation for $H = 0.6$, $\Gamma = 1.9$, $T = 0$, and $\epsilon = 1$ at $\omega = -1.451 + 0.1182i$. The outer curve is for $k_i = 0$, and the inner one is for $k_i = 0.029\,05$.

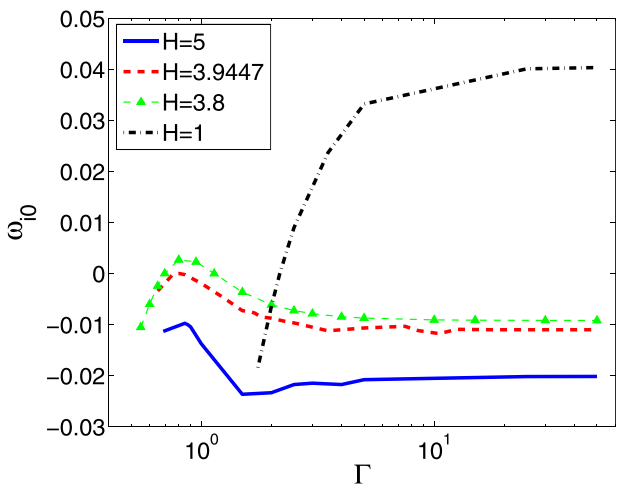

FIG. 12. Range of Γ values under which the flow is absolutely unstable for $H = 5$, 3.9447, 3.8, 1; $\epsilon = 1$, and $T = 0$.

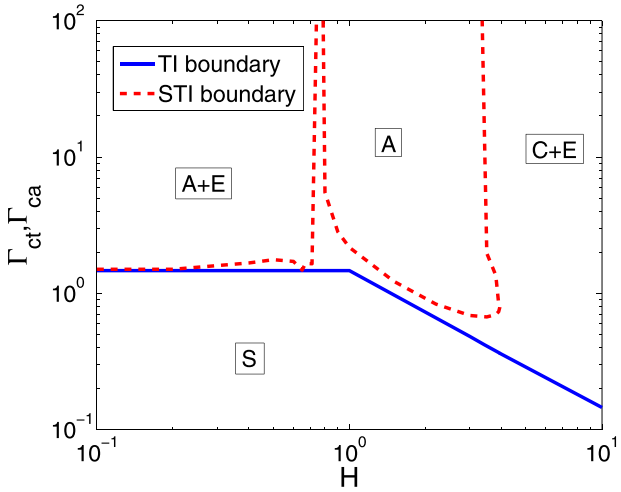

FIG. 13. Absolute instability region for $\epsilon = 1$, $T = 0$ in H–Γ parametric space. In the figure, TI and STI, respectively, stand for temporal and spatio-temporal instability boundaries.

fixed, either absolutely unstable modes or evanescent modes are encountered. In Fig. 13 for $H < 1$ where the short-wave mode is the dominant mode, in temporal instability, for range $H = 0.71$–0.77, only convectively unstable modes or evanescent modes are found.

In Fig. 14, the effect of interfacial tension T on the presence of absolute instability is examined. From temporal stability analysis, it is well-known that T has stabilizing effect on short-wave instability.[5] Hence it is important to understand effect of non-zero T on the existence of absolute instability. Figure 14 shows strong stabilizing effect of T for the onset of absolute instability for $H < 0.77$. Comparing Figs. 13 and 14 for $H < 0.77$, for $T = 0.5$, the absolute instability boundary gets displaced upwards as well as shrinks in terms of H, indicating that, unlike the $T = 0$ case, there is no value of H where the flow undergoes a direct transition from stable modes to absolutely unstable modes. Even here, the "causality competition" takes place between finite-wave mode and short-wave modes, but here it is much severe as the finite-wave mode remains causally legitimate upto a certain value of Γ, and this combined with the formation of evanescent cusps by short-wave mode is the reason that pushes the absolute instability boundary to such high values of Γ_{ca}. The temporal stability analysis shows negligible effect of interfacial tension on finite-wave instability.[5] Figure 14 shows that the non-zero interfacial tension does not have significant effect on the spatio-temporal stability of the finite-wave mode, but has substantial effect on short-wave instability.

2. Plane Poiseuille flow

The velocity profile for plane Poiseuille flow can be obtained by putting $\epsilon = 0$ in Eq. (3) so as to remove the plane Couette component. In this case as well, only a first-order saddle point was observed and hence the procedure of finding absolute instability is the same as in the case of Couette flow. The variation of the critical strain rate, Γ_{ct} and Γ_{ca}, with respect to H for Poiseuille flow is shown in Fig. 15.

Comparing Fig. 13 for Couette flow and Fig. 15, the major difference is the absence of absolute instability for high H, and the cause for this is the absence of finite-wave instability for Poiseuille flow for high H unlike in the case of Couette flow. Also for $H < 1$, the span of the region of absolute instability for Poiseuille flow is smaller than Couette flow for the same value of T. The reason for this result lies in the formation of evanescent cusp points for Poiseuille with relative ease, and the evanescent modes preclude the formation of genuine cusp points. This can be attributed to the complete dominance of the short-wave instability. It is interesting to note the sharp boundary of the absolute instability region at $H \sim 0.15$, and this happens due to the sudden disappearance of genuine cusp formation and appearance of only evanescent cusp formation. Thus, absolute instabilities are not relevant for plane Poiseuille flow.

3. Combined Couette-Poiseuille flow

In the case of the combined Couette-Poiseuille flow depending on the value of ϵ, there are two different classes of

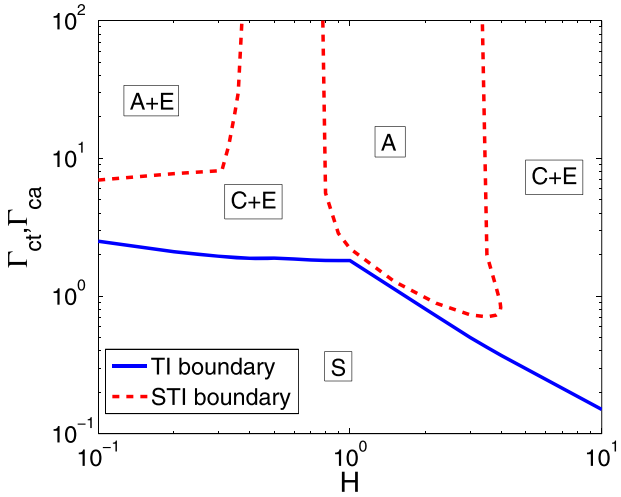

FIG. 14. Absolute instability region for $\epsilon = 1$, $T = 0.5$ in H–Γ parametric space.

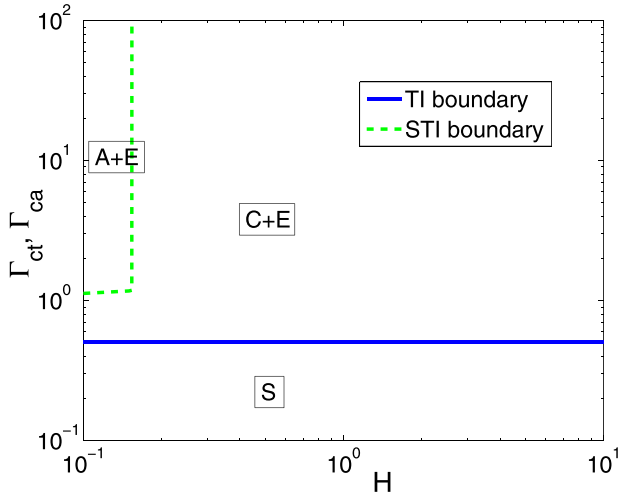

FIG. 15. Temporal and spatio-temporal stability regions for Poiseuille flow with $T = 0$ in H–Γ parameter space.

velocity profiles. Both classes of velocity profiles are considered in the following discussion. Following the same procedure as in the case of Couette flow, we observed the presence of only first-order saddle point for the values of ϵ considered and hence the above methodology for spatio-temporal stability analysis for Couette flow using the Kupfer-Bers and Briggs-Bers methods is applicable. Similar to temporal stability analysis, we study the combined Couette-Poiseuille flow in ϵ–Γ parameter space for the spatio-temporal stability analysis. The absolute instability region is shown in Figs. 16 and 17 alongside temporal stability region so as to compare the two analyses.

Two representative values of H are taken for demonstrating the effect of variation of critical strain rates Γ_{ct} and Γ_{ca} with respect to ϵ for temporal and spatio-temporal stability analysis. We consider $H = 0.1$ as it is the lowest reasonable value of H for which finite-wave temporal instability is completely absent for any value of Γ and for any value of parameter ϵ. We consider $H = 3$ because for $H = 10$ there is no absolute instability even for plane Couette flow.

For $H = 0.1$, the absolute instability and temporal instability curves are parallel to each other as we increase ϵ from 0 to 0.6, and the difference between Γ_{ct} and Γ_{ca} is notable. However, for $0.6 \le \epsilon \le 0.8$, the genuine cusp formation starts to occur for lower values of Γ compared to the results for $\epsilon < 0.6$, thereby reducing the gap between the temporal and spatio-temporal instability boundaries. For the range of ϵ such that $0.8 < \epsilon < 1.1$, both the instability boundaries almost overlap indicating that absolute instability could be realised in experimental studies. This overlapping of the two boundaries occurs once again for $\epsilon > 1.4$ and continues till $\epsilon = 1.5$ for which temporal instability is absent. For region $\epsilon > 1.5$, there is no absolute instability but only convective instability or evanescent cusp formation is predicted.

For $H = 3$, the absolute instability is absent for $\epsilon < 0.8$, but only evanescent cusp points are observed because of the absence of the finite-wave instability. Although for the range $0.8 < \epsilon < 1$ there is the presence of finite-wave instability, the system still does not exhibit absolute instability indicating

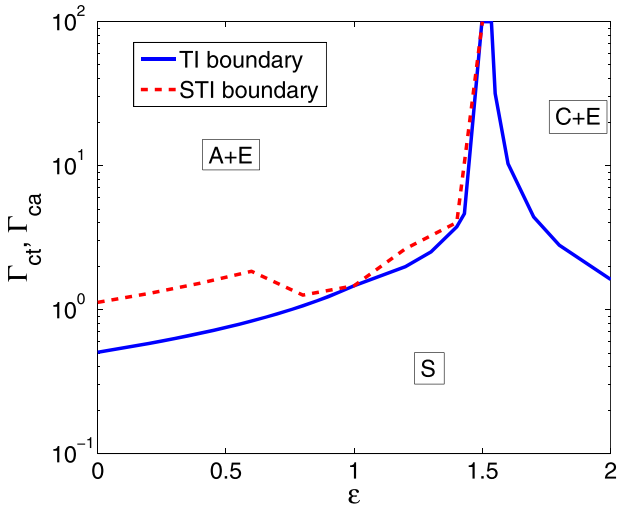

FIG. 16. Absolute and convective instability regions for combined Couette-Poiseuille flow with $T = 0$ in ϵ–Γ parameter space for $H = 0.1$.

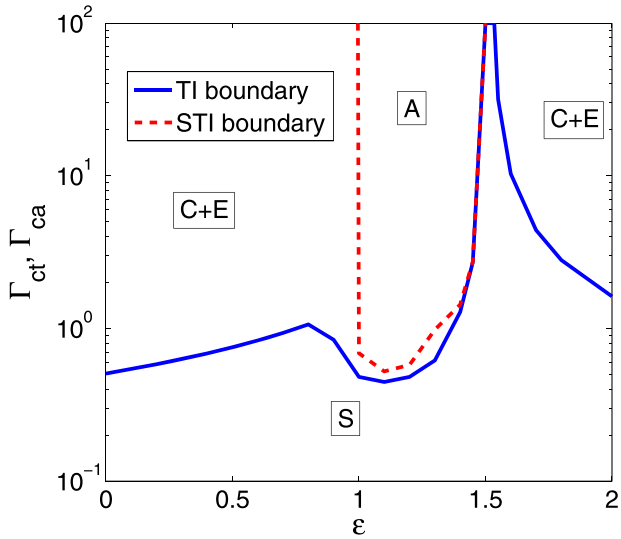

FIG. 17. Absolute and convective instability regions for combined Couette-Poiseuille flow with $T = 0$ in ϵ–Γ parameter space for $H = 3$.

that the presence of finite-wave instability is not a sufficient condition for the presence of absolute instability which was observed in the Couette flow case as well for $H > 3.94$ as shown in Fig. 13. For $\epsilon > 1$, i.e., the combined Couette-Poiseuille flow system with adverse pressure gradients, the system starts exhibiting absolute instability, and it continues till $\epsilon = 1.5$ where the system becomes temporally stable. Similar to the case of $H = 0.1$, for $\epsilon > 1.4$, temporal and spatio-temporal instability boundaries overlap. Also for $\epsilon > 1.5$ as has been observed for the case of $H = 0.1$, there is no absolute instability.

V. CONCLUSIONS

In the present work, we have analyzed the linear temporal and spatio-temporal stability of plane Couette, Poiseuille, and combined Couette-Poiseuille flows of a Newtonian fluid past an incompressible and impermeable neo-Hookean solid in the creeping-flow limit. The temporal instability of the same geometries was studied by Gkanis and Kumar,[7] but due to the use of inconsistent linearized interface conditions, they predicted a finite-wave instability for Poiseuille flow, which is absent in our study. To analyze the effect of change in the pressure gradient in the fluid on the instability, we constructed velocity profiles such that they can continuously vary from Couette flow ($\epsilon = 1$) to intermediate cases, i.e., combined Couette-Poiseuille flow ($0 < \epsilon < 1$ or $\epsilon > 1$ or $\epsilon < 0$) and then to Poiseuille flow ($\epsilon = 0$). In case of the Poiseuille flow, only the short-wave instability is present for any value of H and Γ.

For combined Couette-Poiseuille flow, as ϵ is increased from zero, initially Γ_{ct} increases linearly with ϵ. When ϵ approaches unity, there is a range of ϵ values near unity, where the combined Couette-Poiseuille flow exhibits a finite-wave instability similar to plane Couette flow (and unlike plane Poiseuille flow). For $\epsilon > 1$, the pressure gradient is adverse and acts in a direction opposite to the Couette flow. At a critical value of $\epsilon = 1.5$, the velocity profile has a zero slope at the wall

due to the opposing nature of the pressure-driven and Couette contributions. This removes a crucial coupling between base-state and perturbations that drives the finite-wave instability in plane Couette flow, and hence there is no temporal instability at $\epsilon = 1.5$. However, in the vicinity of $\epsilon = 1.5$, there is a small region where the deformation gradients in the solid are sufficiently small, such that the neo-Hookean solid essentially behaves like a linear elastic solid, and hence exhibit finite wave instability. It must be noted that the previous study of Gkanis and Kumar[7] analyzed the current problem only for $\epsilon < 1.5$. The effect of interfacial tension on the temporal stability was studied in all three geometries, which showed that the stabilizing effect of interfacial tension is more pronounced as ϵ is decreased from 1 to 0. This is because of the dominance of the short-wave instability as ϵ becomes small.

The existence of absolute instability is investigated by using the Kupfer-Bers method[19] after validating the local map $(\omega - \omega_0) \sim (k - k_0)^2$ by obtaining the cusp point in the ω-plane using the images of constant unstable k_i. These cusp points were further verified by obtaining the corresponding pinch point in the k-plane by drawing isocontours of ω_r and ω_i in the k-plane which showed the presence of a first-order saddle point. In some cases, we find the existence of evanescent modes. For Couette flow, it is observed that for $T = 0$ and $T = 0.5$, for $H > 3.94$ and $0.71 < H < 0.77$, the system does not exhibit absolute instability for any value of Γ. For $0.1 < H < 0.71$ and $T = 0$, we find the flow to be absolutely unstable as soon as it becomes temporally unstable thus making absolute instability experimentally relevant. In fact, for $H < 0.4$, $\Gamma_{ca} \sim \Gamma_{ct}$. This indicates that there is a possibility of triggering the absolute instability by selecting this particular H range so as to hasten the transition as the absolute instability is much more catastrophic than the convective instability[34] or may give rise to the global absolute instability.[37] This result could be utilized while designing practical applications of such flows to manipulate the onset of absolute instability. The effect of interfacial tension on the existence of absolute instability is analyzed, and we find a marginal stabilizing effect for high H but is quite strongly stabilizing for low H owing to the presence of the short-wave instability at low H.

The spatio-temporal study of Poiseuille flow showed the presence of absolute instability for $H < 0.15$. The absence of absolute instability for $H > 0.15$ stems from either non-existence of the genuine cusp point or due to the formation of causally legitimate convectively unstable cusp points by finite-wave instability before the short-wave instability. For the combined Couette-Poiseuille flow, the presence of absolute instability was observed for $\epsilon < 1.5$, and for $\epsilon > 1.5$ there is no genuine cusp point. For $H = 0.1$ and $\epsilon > 0.7$, $\Gamma_{ct} \sim \Gamma_{ca}$ making the absolute instability practically relevant. For $H = 3$, the presence of absolute instability is detected only in the region where finite-wave instability is present. Thus, the present study shows for the first time that absolute instabilities are possible in flow through channels with deformable walls (modeled as neo-Hookean solids) at the low Reynolds numbers, and such instabilities can be potentially exploited in improving mixing (even at low Reynolds numbers) in flow through channels with deformable walls.

[1] J. B. Grotberg and O. E. Jensen, "Biofluid mechanics in flexible tubes," Annu. Rev. Fluid Mech. **36**, 121–147 (2004).
[2] T. M. Squires and S. R. Quake, "Microfluidics: Fluid physics at the nanoliter scale," Rev. Mod. Phys. **77**, 977–1026 (2005).
[3] V. Kumaran, G. H. Fredrickson, and P. Pincus, "Flow induced instability of the interface between a fluid and a gel at low Reynolds number," J. Phys. II **4**, 893–904 (1994).
[4] P. Drazin, *Introduction to Hydrodynamic Stability* (Cambridge University Press, Cambridge, 2002).
[5] V. Gkanis and S. Kumar, "Instability of creeping Couette flow past a neo-Hookean solid," Phys. Fluids **15**, 2864–2471 (2003).
[6] Gaurav and V. Shankar, "Stability of pressure-driven flow in a deformable neo-Hookean channel," J. Fluid Mech. **659**, 318–350 (2010).
[7] V. Gkanis and S. Kumar, "Stability of pressure-driven creeping flows in channels lined with a nonlinear elastic solid," J. Fluid Mech. **524**, 357–375 (2005).
[8] Gaurav and V. Shankar, "Stability of fluid flow through deformable neo-Hookean tubes," J. Fluid Mech. **627**, 291–322 (2009).
[9] P. Chokshi and V. Kumaran, "Weakly nonlinear analysis of viscous instability in flow past a neo-Hookean surface," Phys. Rev. E **77**, 056303 (2008).
[10] R. Patne, D. Giribabu, and V. Shankar, "Consistent formulations for stability of fluid flow through deformable channels and tubes," J. Fluid Mech. **827**, 31–66 (2017).
[11] V. Kumaran and R. Muralikrishnan, "Spontaneous growth of fluctuations in the viscous flow of a fluid past a soft interface," Phys. Rev. Lett. **84**, 3310–3313 (2000).
[12] R. Neelamegam, D. Giribabu, and V. Shankar, "Instability of viscous flow over a deformable two-layered gel: Experiment and theory," Phys. Rev. E **90**, 043004 (2014).
[13] M. K. S. Verma and V. Kumaran, "A multifold reduction in the transition Reynolds number, and ultra-fast mixing, in a micro-channel due to a dynamical instability induced by a soft wall," J. Fluid Mech. **727**, 407–455 (2013).
[14] R. Neelamegam and V. Shankar, "Experimental study of the instability of laminar flow in a tube with deformable walls," Phys. Fluids **27**, 024102 (2015).
[15] P. Drazin and W. Reid, *Hydrodynamic Stability* (Cambridge University Press, Cambridge, 1981).
[16] P. Huerre and P. A. Monkewitz, "Local and global instabilities in spatially developing flows," Annu. Rev. Fluid Mech. **22**, 473–537 (1990).
[17] P. J. Schmid and D. S. Henningson, *Stability and Transition in Shear Flows* (Springer, New York, 2001).
[18] R. J. Briggs, *Electron-Stream Interaction With Plasmas* (MIT Press, Cambridge, 1964).
[19] K. Kupfer, A. Bers, and A. K. Ram, "The cusp map in complex-frequency plane for absolute instabilities," Phys. Fluids **30**(10), 3075 (1987).
[20] R. G. Deissler, "The convective nature of instability in plane Poiseuille flow," Phys. Fluids **30**, 2303 (1987).
[21] P. W. Carpenter and A. D. Garrad, "The hydrodynamic stability of flows over Kramer-type compliant surfaces. Part 1. Tollmien-Schlichting instabilities," J. Fluid Mech. **155**, 465–510 (1985).
[22] P. K. Sen and D. S. Arora, "On the stability of laminar boundary-layer flow over a flat plate with a compliant surface," J. Fluid Mech. **197**, 201–240 (1988).
[23] K. S. Yeo, B. C. Khoo, and H. Z. Zhao, "The absolute instability of boundary-layer flow over viscoelastic walls," Theor. Comput. Fluid Dyn. **8**, 237–252 (1996).
[24] K. S. Yeo, B. C. Khoo, and H. Z. Zhao, "The convective and absolute instability of fluid flow over viscoelastic compliant layers," J. Sound Vib. **223**(3), 379–398 (1999).
[25] K. S. Yeo, B. C. Khoo, and H. Z. Zhao, "Turbulent boundary layer over a compliant surface: Absolute and convective instabilities," J. Fluid Mech. **449**, 141–168 (2001).
[26] M. Hamadiche and M. Gad-el Hak, "Spatiotemporal stability of flow through collapsible, viscoelastic tubes," AIAA J. **42**(4), 772 (2004).
[27] M. Hamadiche, N. Kizilova, and M. Gad-el Hak, "Suppression of absolute instabilities in the flow inside a compliant tube," Commun. Numer. Methods Eng. **25**, 505–531 (2009).
[28] G. A. Holzapfel, *Nonlinear Solid Mechanics* (John Wiley, Chichester, UK, 2000).
[29] C. Macosko, *Rheology: Principles, Measurements, and Applications* (VCH, New York, 1994).

[30]L. E. Malvern, *Introduction to the Mechanics of a Continuous Medium* (Prentice-Hall, Englewood Cliffs, NJ, 1969).
[31]C. M. Bender and S. A. Orszag, *Advanced Mathematical Methods for Scientists and Engineers I: Asymptotic Methods and Perturbation Theory* (Springer, New York, 1999).
[32]R. J. Ablowitz and A. S. Fokas, *Complex Variables: Introduction and Applications* (Cambridge University Press, Cambridge, 2003).
[33]V. Kumaran, "Stability of the viscous flow of a fluid through a flexible tube," J. Fluid Mech. **294**, 259–281 (1995).
[34]R. J. Lingwood, "Absolute instability of the boundary layer on a rotating disc," J. Fluid Mech. **299**, 17–33 (1995).
[35]W. Koch, "Direct resonances in Orr-Sommerfeld problems," Acta Mech. **59**, 11–29 (1986).
[36]D. S. Henningson, A. Lundbladah, and A. V. Johansson, "A mechanism for bypass transition from localized disturbances in wall-bounded shear flows," J. Fluid Mech. **250**, 169–207 (1993).
[37]J. M. Chomaz, P. Huerre, and L. G. Redekopp, "Bifurcations to local and global modes in spatially-developing flow," Phys. Rev. Lett. **60**, 25 (1988).